Aalborg Universitet

AALBORG UNIVERSITY
DENMARK

Flow structures and heat transfer in repeating arrangements of staggered rectangular winglet pairs by Large Eddy Simulations

Effect of winglet height and longitudinal pitch distance

Bjerg, Allan; Christoffersen , Kristian Boe; Sørensen, Henrik; Hærvig, Jakob

Published in:
International Journal of Heat and Mass Transfer

DOI (link to publication from Publisher):
10.1016/j.ijheatmasstransfer.2018.11.015

Creative Commons License
CC BY-NC-ND 4.0

Publication date:
2019

Document Version
Accepted author manuscript, peer reviewed version

Link to publication from Aalborg University

Citation for published version (APA):
Bjerg, A., Christoffersen , K. B., Sørensen, H., & Hærvig, J. (2019). Flow structures and heat transfer in repeating arrangements of staggered rectangular winglet pairs by Large Eddy Simulations: Effect of winglet height and longitudinal pitch distance. *International Journal of Heat and Mass Transfer*, *131*, 654-663. https://doi.org/10.1016/j.ijheatmasstransfer.2018.11.015

General rights
Copyright and moral rights for the publications made accessible in the public portal are retained by the authors and/or other copyright owners and it is a condition of accessing publications that users recognise and abide by the legal requirements associated with these rights.

- Users may download and print one copy of any publication from the public portal for the purpose of private study or research.
- You may not further distribute the material or use it for any profit-making activity or commercial gain
- You may freely distribute the URL identifying the publication in the public portal -

Take down policy
If you believe that this document breaches copyright please contact us at vbn@aub.aau.dk providing details, and we will remove access to the work immediately and investigate your claim.

Flow structures and heat transfer in repeating arrangements of staggered rectangular winglet pairs by Large Eddy Simulations: Effect of winglet height and longitudinal pitch distance

A. Bjerg[a], K. Christoffersen[a], H. Sørensen[a], J. Hærvig[a]

[a] *Aalborg University, Department of Energy Technology, Pontoppidanstræde 111, DK-9220 Aalborg, Denmark*

Abstract

Large Eddy Simulations (LES) of the flow in repeating arrangements of staggered rectangular winglet pairs are presented to get a better understanding of the detailed flow and heat transfer enhancing mechanisms. Simulations are performed for various geometrical configurations with the winglet height h and longitudinal pitch distance L_p being varied in the ranges $h/H \in [0.3; 0.7]$ and $L_\mathrm{p}/H \in [3; 7]$ at $\mathrm{Re} = u_\mathrm{b}H/\nu = 700$ and $\mathrm{Pr} = 0.71$.

The results show that three different types of vortices are generated by the winglet pairs: main longitudinal vortices, corner vortices and induced vortices, with the main longitudinal vortices being the main contributor to heat transfer enhancement. It is found that the heat transfer and pressure loss increase with increasing winglet height and decrease with increasing longitudinal pitch distance. The winglet height proves to have the highest impact on both the heat transfer and pressure loss. Furthermore, the results show that local heat transfer can effectively be increased on the fin side by utilising smaller winglet heights. For higher winglet heights local heat transfer is observed to be more equally distributed on both sides.

Overall, pressure loss increments f/f_0 between 3.3 and 33.5 and heat transfer enhancements $\mathrm{Nu}/\mathrm{Nu}_0$ between 2.2 and 4.6 are found. When introducing the performance factor $\eta = (\mathrm{Nu}/\mathrm{Nu}_0)/(f/f_0)^{1/3}$ as a measure for heat transfer enhancement relative to pressure loss, the optimal geometries generally have a combination of lower winglet heights and higher longitudinal pitch distances.

Keywords: Rectangular winglet pairs, Vortex generator, Parametric variation, Winglet height, Longitudinal pitch distance, Large Eddy Simulation (LES), Periodic flow

1. Introduction

In recent decades, considerable attention has been devoted to heat transfer enhancement in compact heat exchangers. Compact heat exchangers are widely used across industries such as in refrigeration, airconditioning, electronics cooling and aerospace applications [1]. Several different flow manipulation techniques can be applied to enhance heat transfer, and these are generally divided into two categories; active and passive methods [2–4]. Passive methods have proven popular since they do not require external power, are reliable, cheap and easily applicable. One of the promising passive methods for heat transfer enhancement is vortex generators. Vortex generators are special flow obstructions inserted into the flow field to create vortices that promote mixing and thereby enhance heat transfer. However, this comes with a penalty in terms of an increased pressure loss.

Due to the wide range of parameters describing the vortex generator geometry, it is not straight

Email address: abe@et.aau.dk (A. Bjerg)

© 2018. This manuscript version is made available under the CC-BY-NC-ND 4.0 license http://creativecommons.org/licenses/by-nc-nd/4.0/

forward to design them. Biswas et al. [5] and Biswas and Chattopadhyay [6] numerically investigated the effect of angle of attack on heat transfer enhancement using mounted and punched delta wings in a rectangular channel. Heat transfer enhancement was found to be primarily caused by the longitudinal vortices generated by the wing. The loss coefficient and Nusselt number increased with increasing angle of attack. Increase in Nusselt number of 34 % and loss coefficient of 79 % were found for the mounted wing. For the punched wing, the Nusselt number and loss coefficient increase were 10 % and 48 %, respectively. Tiggelbeck et al. [7, 8] experimentally investigated the effect of angle of attack on heat transfer enhancement for double rows of staggered and aligned delta winglet pairs in a channel flow. It was found that an angle of attack of 45° proved better for heat transfer enhancement yielding a global enhancement of 80 %. The second row of vortex generators was found to increase flow unsteadiness and therefore working as a booster for heat transfer enhancement. No significant changes were found between the staggered and aligned configuration. Tiggelbeck et al. [9] expanded upon the previous work by investigating four different vortex generator geometries, namely delta- and rectangular wing and winglet pairs. Winglets proved to perform better than wings and an optimum angle of attack for heat transfer enhancement was found to lie between 45° and 65°. Beside the above, several authors were found to agree that heat transfer enhancement and pressure loss increase with increasing angle of attack [1, 10–13]. However, supporting the findings of Tiggelbeck et al. [7, 8, 9], Ferrouillat et al. [14] found that in terms of performance, angles of attack above 65° are not efficient. This is because mainly transverse vortices are being generated above $\alpha = 65°$ leading to a significant increase in pressure loss relative to heat transfer enhancement. This is further supported by the findings of Wu and Tao [15, 16], Fiebig [17] and Abdollahi and Shams [18] stating that $\alpha = 45°$ provided a peak in the heat transfer enhancement. In this regard, Abdollahi and Shams [18] found that $\alpha = 45°$ leads to higher fluid mixing and thinner thermal boundary layer yielding a higher heat transfer enhancement compared to other angles of attack in the range between 15° and 90°. Additionally, Fiebig [19] numerically investigated flow structures related to heat transfer enhancement in a low Reynolds number channel flow with periodic rectangular winglet pairs ($\alpha = 45°$) and transverse ribs ($\alpha = 90°$). The winglet pairs mainly generated longitudinal vortices while the transverse ribs generated transverse vortices. It was found that the longitudinal vortices were better for heat transfer enhancement due to their spiralling energy transport in the streamwise direction. Self-sustained oscillations were generated at a lower Reynolds number for the transverse vortices compared to the longitudinal vortices, however, at Re = 350 the heat transfer enhancement was almost the same for both configurations but with the rectangular winglet pairs causing only half the pressure loss. A similar conclusion was drawn by Liu et al. [20] who investigated flow and heat transfer in microchannels with different configurations of rectangular winglet pairs. The critical Reynolds numbers for the laminar-to-turbulent transition were found to be in the range between 600 and 720 which is significantly lower than for a plane channel (Re $\approx$ 2300).

Through the literature it is evident that the effect of Reynolds number have been studied frequently. Several authors agree that heat transfer enhancement and pressure loss increase with Reynolds number [1, 7–9, 12, 15, 16]. The heat transfer enhancement due to increasing Reynolds number is associated with the size and strength of the generated vortices increase with increasing Reynolds number [12, 13, 21, 22]. As the Reynolds number increases, corresponding to a fully turbulent channel flow, Zhu et al. [23] found for Re = $50,000$ that the use of vortex generators is inefficient. It was found that the mean heat transfer enhancement was 16-19 % with corresponding pressure loss of 400-500 %.

Configurations generating counter-rotating vortices have been found to be more effective for heat transfer enhancement than co-rotating configurations [10, 24, 25]. Several different configurations were investigated by Sinha et al. [25] where the

counter-rotating configurations proved most effective. Additionally, Tian et al. [26] found that rectangular winglets in a common-flow-down configuration had a better overall performance than in a common-flow-up configuration. Sinha et al. [25] also investigated aligned and staggered arrangements of delta winglets which showed that the staggered arrangement performed better in terms of heat transfer enhancement and pressure loss. A similar conclusion was drawn by Chen et al. [27] where the staggered arrangement showed a 20 % higher heat transfer enhancement and 14.5 % lower pressure loss than the aligned arrangement. Dupont et al. [21] experimentally studied the effect of a four-row-four-column arrangement of embossed rectangular winglet pairs. Similar to the findings of Tiggelbeck et al. [7, 8] the consecutive rows increase flow unsteadiness and works as a booster for heat transfer enhancement. It was found that a saturation of the vortex strength and size took place after the third row. Furthermore, the turbulence development was accelerated by the vortex generators and for Re $>$ 2000 the maximum turbulence level was reached after the first row. Several other geometrical changes have been studied. Turk and Junkhan [28], Torii and Yanagihara [11], Li et al. [29] and Wu and Tao [15, 16] studied the effect of changing the winglet height. Common findings were that the heat transfer enhancement and pressure loss increased with increasing winglet height. According to Li et al. [29], the higher winglets create a larger low pressure region downstream and thus stronger vortices are formed which carry heat from the high temperature regions to the low temperature regions more effectively. Additionally,the pressure loss was found to be particularly sensitive to changes in winglet height. In this regard, Wu and Tao [15, 16] suggested to increase length and decrease height for constant vortex generator area. Further parametric variations by Wu and Tao [15, 16] showed that heat transfer enhancement decreased with decreasing transverse winglet pair spacing. Sohankar and Davidson [1] investigated the impact of changing the thickness of a rectangular winglet pair. It was found that thicker vortex generators form stronger and larger longitudinal vortices giving rise to higher heat transfer enhancement. Similar results were found for thick vortex generators with lower angle of attack and thin vortex generators with higher angle of attack.

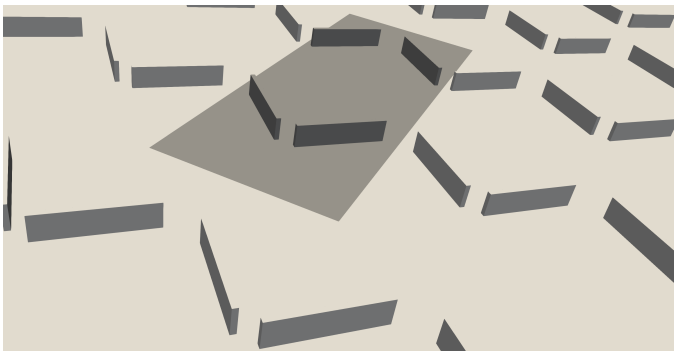

Fig. 1. Overview of the repeatable geometry consisting of staggered arrangements of rectangular winglet pair vortex generators with one repeatable section highlighted.

As stated by Sinha et al. [25], little to no research has been carried out on staggered arrangements of vortex generators. Therefore, the present work focuses on heat transfer enhancement in repeating staggered arrangements of rectangular winglet pair vortex generators (see Fig. 1). Flow structures due to changes in winglet height h and longitudinal pitch distance L_p, see Fig. 2, and their impact on heat transfer and pressure loss are investigated. To get a better understanding of the detailed heat transfer mechanisms, this study presents Large Eddy Simulations (LES) that resolve the larger eddies important for heat transfer enhancement. Focus is on a flow of dry air with $\mathrm{Re} = u_\mathrm{b}H/\nu = 700$ and $\mathrm{Pr} = 0.71$.

2. Governing equations and numerical details

2.1. Computational domain

Fig. 2 shows the computational domain along with the different parameters used to describe the geometry. Table 1 lists the different parameters in Fig. 2.

2.2. Governing equations

The Large Eddy Simulations (LES) are governed by the time-dependent space-filtered Navier-Stokes equations. The space-filtered momentum-

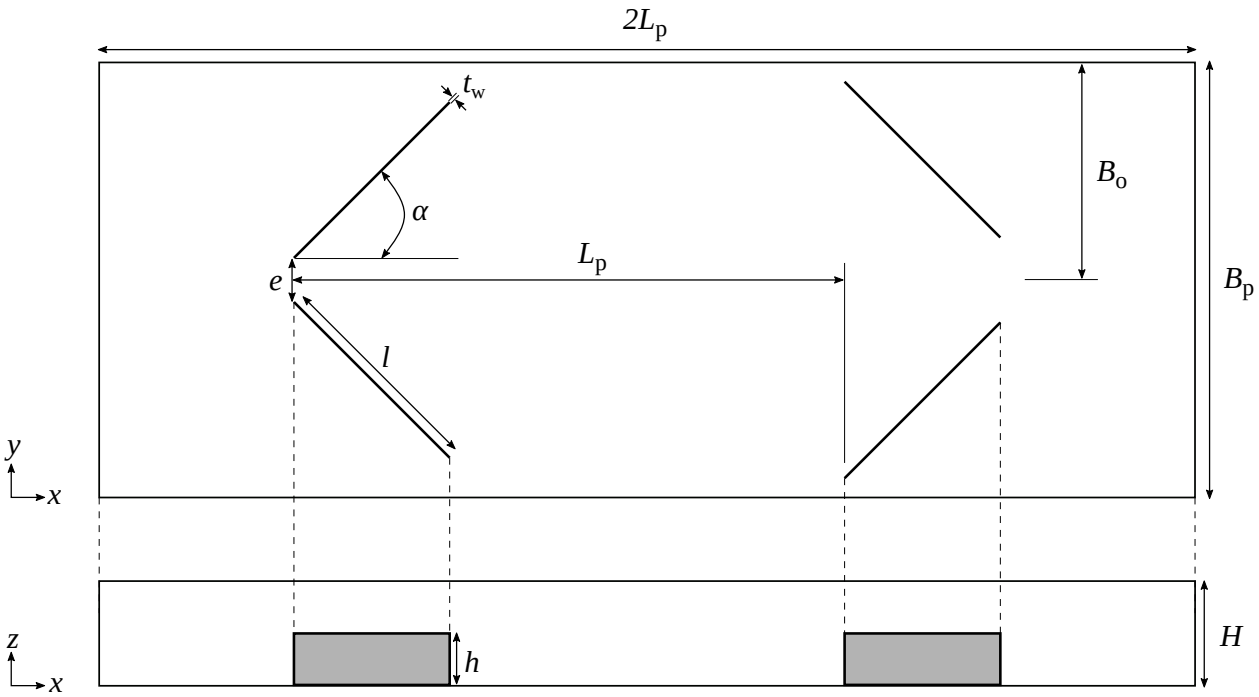

Fig. 2. Schematic of the computational domain with staggered rectangular winglet pair vortex generators. The different geometrical properties along with their values are given in Table 1. The winglet pair centre tip distance e is measured between the centres of the leading edges of the winglets.

Table 1. Geometrical properties for the computational domain configuration shown in Fig. 1 and 2. This is referred to as the standard configuration.

H	Domain height	$1H$
B_o	Staggered offset	$2H$
B_p	Transverse pitch distance	$4H$
e	Winglet pair centre tip distance	$0.4H$
h	Winglet height	$0.5H$
l	Winglet length	$2H$
L_p	Longitudinal pitch distance	$5H$
t_w	Winglet thickness	$0.1H$
α	Angle of attack	45°

and temperature equations for a three-dimensional incompressible viscous flow are given in Eq. (1) and (2):

$$\frac{\partial \bar{u}_i}{\partial t} + \frac{\partial \left(\bar{u}_i \bar{u}_j\right)}{\partial x_j} = -\frac{1}{\rho}\frac{\partial \bar{P}}{\partial x_i} + \frac{\partial}{\partial x_j}\left[\left(\nu + \nu_t\right)\frac{\partial \bar{u}_i}{\partial x_j}\right] + \beta\delta_{1i} \tag{1}$$

$$\frac{\partial \bar{T}}{\partial t} + \frac{\partial \left(\bar{u}_j \bar{T}\right)}{\partial x_j} = \frac{\partial}{\partial x_j}\left[\left(\frac{\nu}{\mathrm{Pr}} + \frac{\nu_t}{\mathrm{Pr}_t}\right)\frac{\partial \bar{T}}{\partial x_j}\right] - \gamma \bar{u}_1 \tag{2}$$

In these equations, the i and j indices denote the x-, y- or z-component of the velocity or coordinate axis. For clarity $x_x = x$, $x_y = y$ and $x_z = z$. The turbulent Prandtl number is constant at $\mathrm{Pr}_t = 0.85$.

Since the flow in the majority of the channel is both thermally and hydro-dynamically fully developed, attention is devoted to this part of the channel. Therefore, periodic boundary conditions are applied in the streamwise and spanwise direction. These are applied according to the approach suggested by Patankar et al. [30], which is shown by Hærvig et al. [31] to give resonable results when compared to experiments. Thus, β and γ are added to the governing equations, representing the streamwise driving pressure gradient and temperature gradient, respectively. This means that the pressure and temperature solved in Eq. (1) and (2) are the periodic parts. For the case of constant wall heat flux, γ is defined as

$\gamma = \dot{q}/Hc_{\mathrm{p}}u_{\mathrm{b}}\rho$. To achieve the desired Reynolds number, β is dynamically adjusted to obtain the desired bulk velocity u_{b}. The bulk velocity is defined as:

$$u_{\mathrm{b}}(x) = \frac{\int u(x,y,z)dA}{A(x)} \tag{3}$$

from which the bulk temperature, T_{b}, can be calculated as:

$$T_{\mathrm{b}}(x) = \frac{\int T(x,y,z)u(x,y,z)dA}{u_{\mathrm{b}}(x)A(x)} \tag{4}$$

Note that T_{b} remains constant along the streamwise position x due to the last term in Eq. (2).

The finite volume method is used to discretise the governing equations. The second-order Crank-Nicolson scheme is used for temporal discretisation and the second-order central differencing scheme is used for spatial discretisation, as suggested by Davidson [32]. A 0.1 Euler blending is added to the temporal scheme for robustness. The pressure-velocity coupling is done using the Pressure-Implicit with Splitting of Operators (PISO) algorithm which is run with an adjustable time step to obtain a Courant number of 0.85, as suggested by Mirzaei et al. [33]. The subgrid-scale (sgs) stresses are modelled using the Wall-Adapting Local Eddy-viscosity (WALE) model proposed by Nicoud and Ducros [34]. The WALE model is well-suited for wall-bounded flows since the eddy viscosity ν_{t} naturally goes to zero in the vicinity of the wall. Therefore, no damping functions are needed for wall-bounded flows. The constant C_ω is set to 0.325 [33].

2.3. Non-dimensional groups

The heat transfer and pressure loss are evaluated using dimensionless parameters, namely the Nusselt number Nu and the loss coefficient f. By combining Newton's law of cooling and Fourier's law of heat conduction with the general definition of the Nusselt number, an expression for the global Nusselt number is obtained and given in Eq. (5):

$$\mathrm{Nu} = -\frac{\partial T}{\partial n}\frac{H}{\Delta T} \tag{5}$$

where $\partial T/\partial n$ is the wall normal temperature gradient area-averaged over all wall faces and $\Delta T = T_{\mathrm{w}} - T_{\mathrm{b}}$ is the temperature difference between the wall temperature and the fluid bulk temperature. The loss coefficient is calculated as defined in Eq. (6) as suggested by Esmaeilzadeh et al. [35]:

$$f = \frac{H}{0.5\rho u_b^2}\frac{\partial P}{\partial x} \tag{6}$$

where $\partial P/\partial x$ is the streamwise pressure gradient across the computational domain. As a measure of performance accounting for both heat transfer and pressure loss for equal pumping power, the performance factor in Eq. (7), η, suggested by Webb and Eckert [36] is used:

$$\eta = \frac{\mathrm{Nu}/\mathrm{Nu}_0}{(f/f_0)^{1/3}} \tag{7}$$

where Nu_0 and f_0 are the benchmark values obtained from a simulation without winglets (i.e. $h/H = 0$) and with periodic boundary conditions in the streamwise and spanwise directions.

3. Grid verification

The computational domain is discretised using a structured grid with hexahedral cells. The overall grid topology is visualised in Fig. 3. To achieve a proper near-wall resolution, the wall-adjacent cells are sized to obtain $y^+ \approx 1$. To determine a sufficient grid resolution, a grid convergence study is conducted on the standard configuration. Three different grid sizes are generated

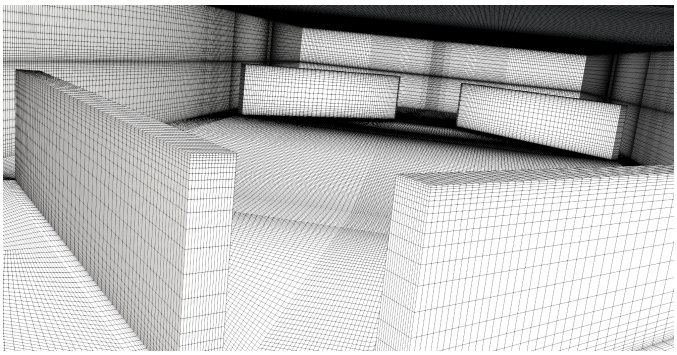

Fig. 3. Overview of the structured grid used for the simulations.

by doubling the number of cells, which results in grid sizes of 1.1, 2.2 and 4.4 million cells. The exact numerical solution is estimated using Richardson's extrapolation and the Grid Convergence Index (GCI) suggested by Roache [37]. From the GCI, an error band is obtained as $f_\mathrm{e} \pm f_\mathrm{e} \cdot \mathrm{GCI}_{12}$, where f_e is the estimated exact solution and 1 and 2 denotes grid 1 and 2. The GCI is given as:

$$\mathrm{GCI} = \frac{F_\mathrm{s}|\epsilon|}{r^p - 1} \tag{8}$$

where F_s is a safety factor, ϵ is the relative error between the two grids, r is the grid refinement ratio and p is the order of convergence. The sensitivity of changes in grid resolution on the Nusselt number Nu and the loss coefficient f are shown in Fig. 4 and 5, respectively, along with the estimated exact solution and the error band estimated using a safety factor $F_\mathrm{s} = 1.25$ as suggested by Roache [37]. Furthermore, the effect of changes in grid resolution on local heat transfer is shown in Fig. 6 by means of the time-averaged wall normal temperature gradient $\langle \partial T/\partial n \rangle$ at the lower wall. This is to make sure that the larger eddy scales important for heat transfer enhancement are resolved sufficiently.

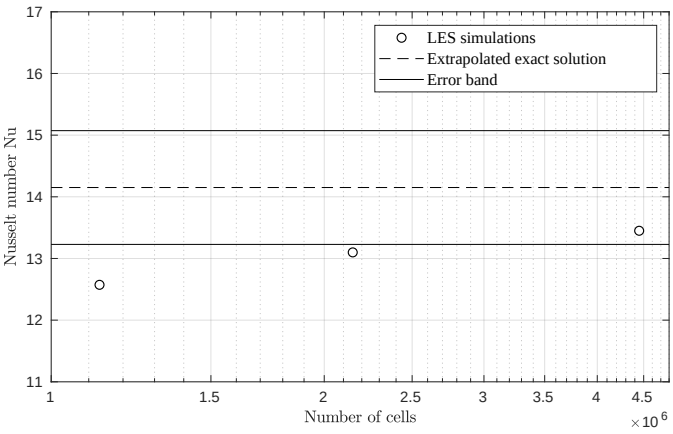

Fig. 4. Sensitivity of changes in the grid resolution on the Nusselt number Nu. The estimated exact solution is shown with a dashed line. The solid lines illustrate the error band based on a safety factor $F_\mathrm{s} = 1.25$, see Eq. (3).

As Fig. 4 and 5 show, both the loss coefficient f and the Nusselt number Nu are within the error band obtained with a safety factor $F_\mathrm{s} = 1.25$

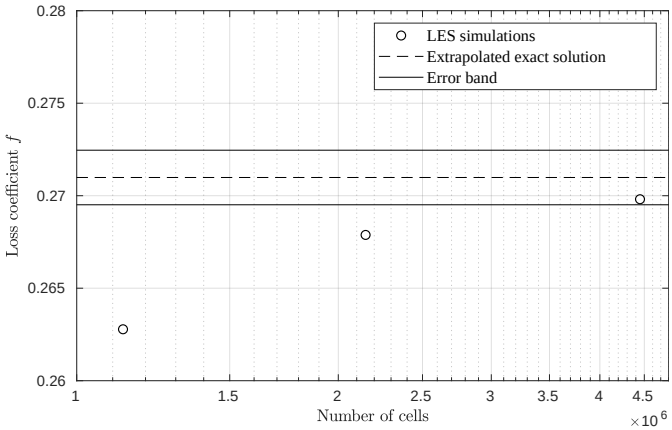

Fig. 5. Sensitivity of changes in the grid resolution on the loss coefficient f. The estimated exact solution is shown with a dashed line. The solid lines illustrate the error band based on a safety factor $F_\mathrm{s} = 1.25$, see Eq. (3).

for the grid with 4.4 million cells. This is further supported by Fig. 6, which shows an overall small difference in the time-averaged wall normal temperature gradient between the grids with 2.2 and 4.4 million cells. This suggests that the larger eddy scales important for heat transfer enhancement are resolved sufficiently using the grid with 4.4 million cells. For this grid, the cell density along the winglets are 63 cells/l.

The grid quality in terms of cell angles is evaluated using orthogonal quality and equiangular skewness defined as:

$$\text{Orthogonal quality} = \min\left[\frac{\boldsymbol{A}\cdot\boldsymbol{f}}{|\boldsymbol{A}||\boldsymbol{f}|}, \frac{\boldsymbol{A}\cdot\boldsymbol{c}}{|\boldsymbol{A}||\boldsymbol{c}|}\right] \tag{9}$$

$$\text{Equiangular skewness} = \max\left[\frac{\theta_\mathrm{max} - \theta_\mathrm{e}}{180^\circ - \theta_\mathrm{e}}, \frac{\theta_\mathrm{e} - \theta_\mathrm{min}}{\theta_\mathrm{e}}\right] \tag{10}$$

where $\theta_\mathrm{e} = 90^\circ$ for hexahedral cells. In Eq. (9), $\boldsymbol{A}$ is the face normal vector, $\boldsymbol{f}$ is a vector from the centre of the cell to the centre of that face and $\boldsymbol{c}$ is a vector from the centre of the cell to the cell centre of the adjacent cell that shares the face. Fig. 7 and Fig. 8 show the distributions of the orthogonal quality and equiangular skewness for the grid independent mesh. For the orthogonal quality a value of 1 is best and from Fig. 7 it is shown that 76.3 % of the cells have an orthogonal quality above 0.9. Fig. 8 show that 73.3 % of the

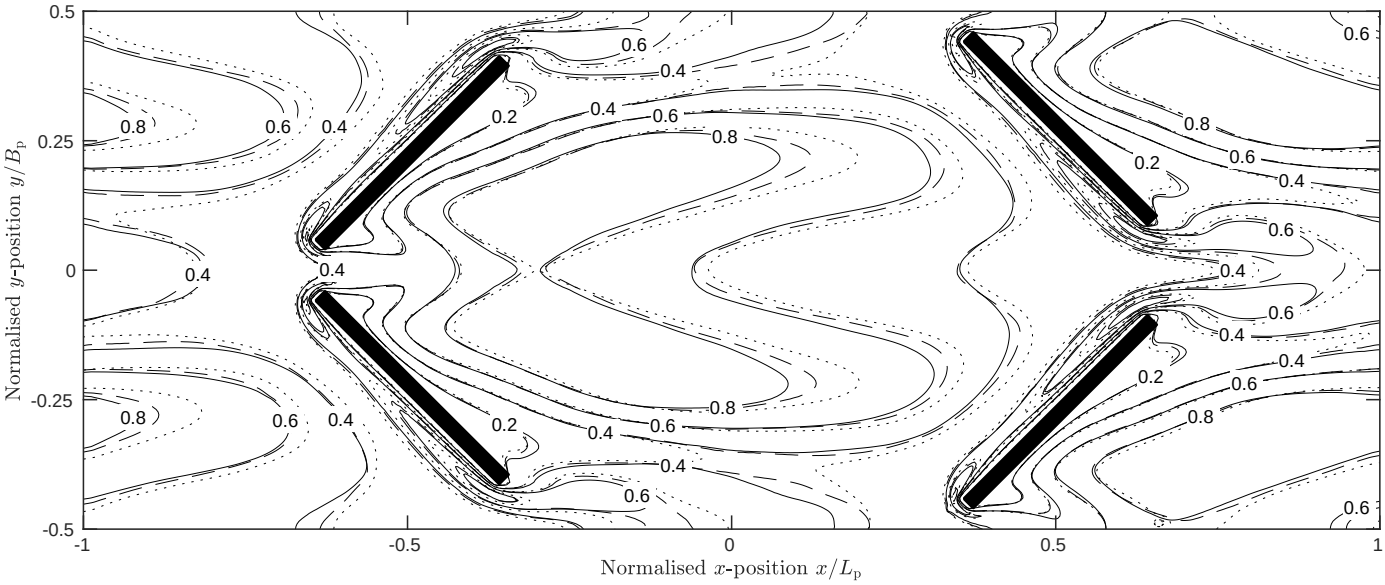

Fig. 6. Effect of changes in grid resolution on local heat transfer visualised by contours of the normalised time-averaged wall normal temperature gradient $\langle \partial T/\partial n \rangle$ at the lower wall. For normalisation the maximum time-averaged wall normal temperature gradient across the different cases is used. (· · ·) 1.1 million cells; (- - -) 2.2 million cells; (——) 4.4 million cells.

cells are of high quality and have an equiangular skewness below 0.25. This mesh is therefore used for all the cases with different longitudinal pitch distances L_p and winglet heights h.

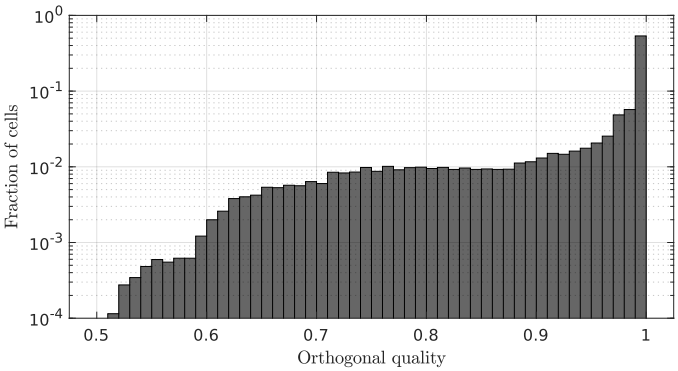

Fig. 7. Orthogonal quality distribution for the grid independent mesh.

4. Results and discussion

To systematically investigate a wide range of possible geometries, the winglet height h and longitudinal pitch distance L_p are varied in the ranges $h/H \in [0.3; 0.7]$ and $L_p/H \in [3; 7]$ in step sizes of 0.1 and 1.0, respectively. Fig. 9 and 10 show the heat transfer and pressure loss enhancements in

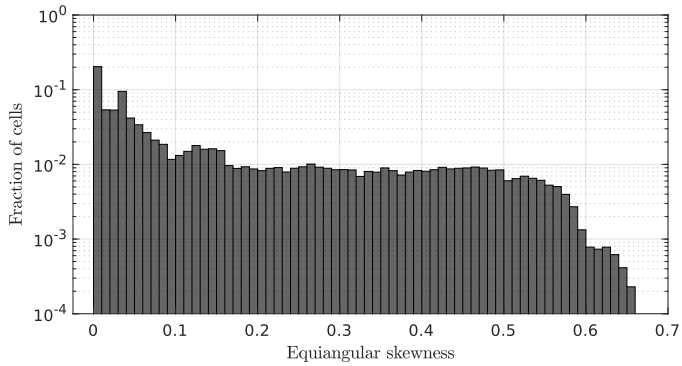

Fig. 8. Equiangular skewness distribution for the grid independent mesh.

terms of $\mathrm{Nu}/\mathrm{Nu}_0$ and f/f_0 resulting from the geometrical variations. It is evident from Fig. 9 and 10 that the heat transfer enhancement and pressure loss increase follow the same tendency. Both increase with increasing winglet height and decrease with increasing longitudinal pitch distance. Similar tendencies were found in the parametric study conducted by Wu and Tao [16]. As expected, heat transfer enhancement $\mathrm{Nu}/\mathrm{Nu}_0$ and pressure loss increase f/f_0 approach unity as $h/H \rightarrow 0$ or $L_p \rightarrow \infty$, which in both extremes correspond to the benchmark configuration. Furthermore, the figures show that the winglet height has

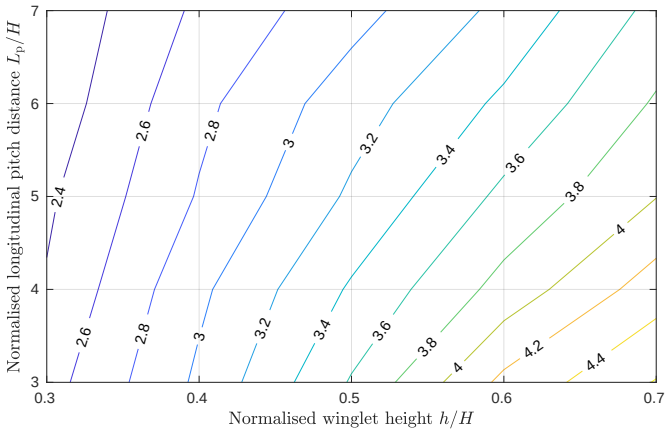

Fig. 9. Contours of heat transfer enhancement $\mathrm{Nu}/\mathrm{Nu}_0$ at varying normalised winglet heights h/H and longitudinal pitch distances L_p/H.

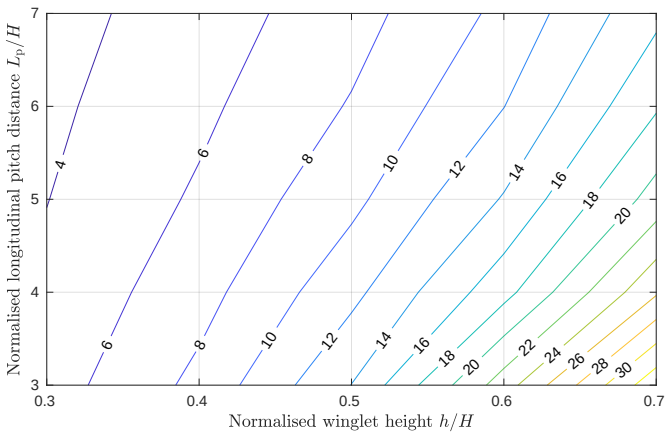

Fig. 10. Contours of pressure loss increase f/f_0 at varying normalised winglet heights h/H and longitudinal pitch distances L_p/H.

the largest impact on both the pressure loss and the heat transfer enhancement within the investigated range. For the pressure loss, this is immediately a consequence of a higher form drag resulting from the higher blockage ratio as the winglet height increases. Additionally, the impact of the longitudinal pitch distance is more significant at larger winglet heights. Fig. 11 shows the performance factor η as function of the winglet height and longitudinal pitch distance. The highest performance factors are in general obtained for configurations with low winglet heights and high longitudinal pitch distances. This agrees with the findings of Tiggelbeck et al. [7, 8] and Ferrouillat et al. [14] who found optimum consecutive row distances of 7-10 times the channel height.

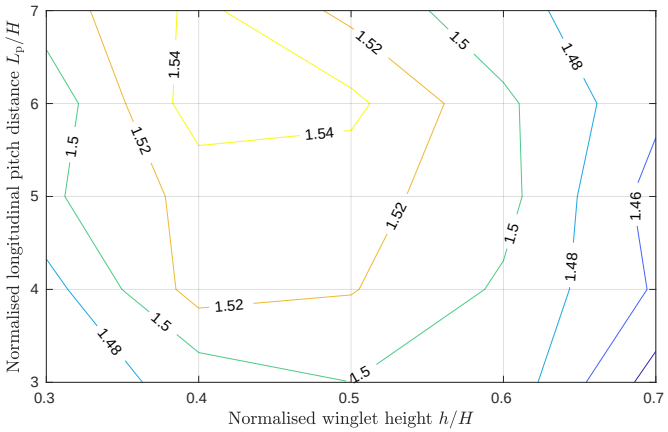

Fig. 11. Contours of performance factor $\eta = (\mathrm{Nu}/\mathrm{Nu}_0)/(f/f_0)^{1/3}$ at varying normalised winglet heights h/H and longitudinal pitch distances L_p/H.

To better understand the main flow mechanisms leading to heat transfer enhancement, the following section presents an overview and discussion of the detailed flow phenomena occurring in the channel.

4.1. Flow characteristics

The vortex structures generated downstream the winglets (see Fig. 12) are of interest to better understand the variations in heat transfer and pressure loss reported in the previous section. The vortex structures are divided into three categories: main longitudinal vortices, corner vortices and induced vortices. Similar vortex structures were found to be generated by the vortex generators in the study by Sohankar and Davidson [1].

Main longitudinal vortices

Fig. 12 shows the main longitudinal vortices. The main longitudinal vortices form due to flow separation occurring over and around the winglets. These vortices are largest in size and strength and persist well downstream. Therefore, the main longitudinal vortices are the main contributor to heat transfer enhancement in the domain. Furthermore, the vortices move towards the sides of the domain in the downstream region. This is in agreement with the findings of Tian et al. [26] on rectangular winglet pairs in a common-flow-down configuration.

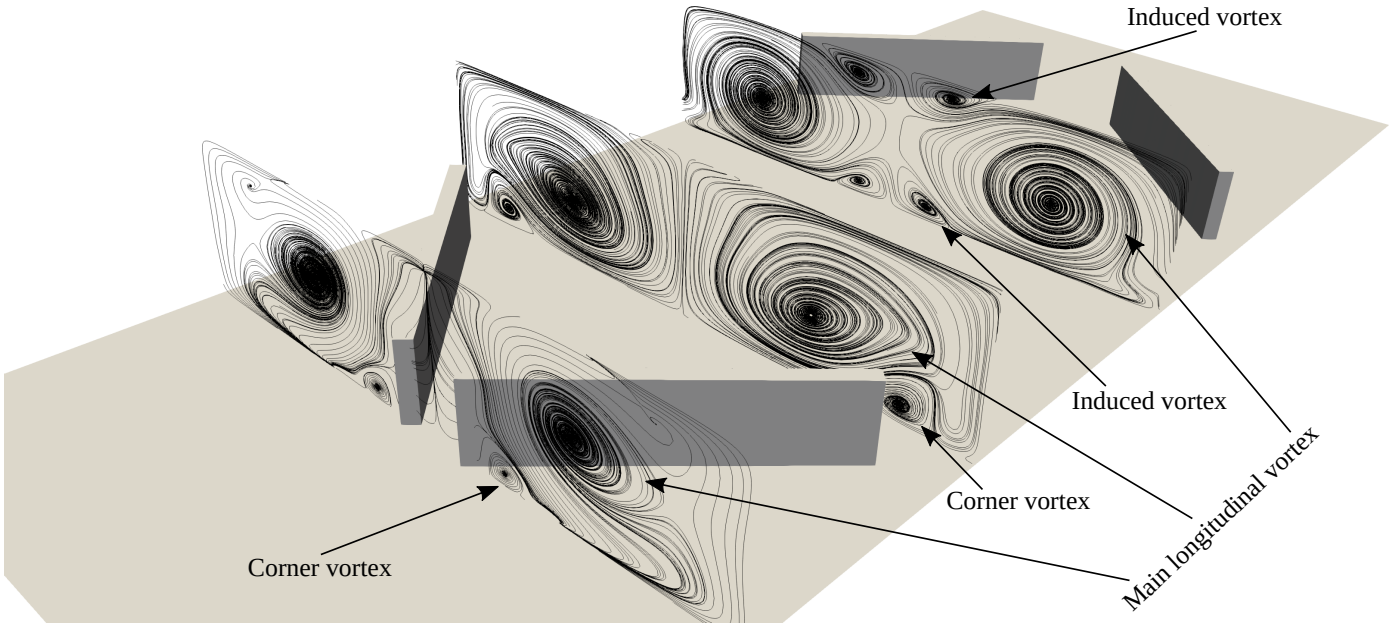

Fig. 12. Streamlines of the time-averaged flow field at different streamwise locations showing the main longitudinal vortices, corner vortices and induced vortices.

Corner vortices

Fig. 12 shows the corner vortices. Corner vortices form near the wall at the lower part of the winglet leading edge due to a pressure gradient towards the lower wall. The pressure gradient occurs as the fluid approaches stagnation near the winglet leading edge. The corner vortices are present along the upstream side of the winglets and are carried downstream at the trailing edge. However, they are smaller in size and strength compared to the main longitudinal vortices and are more susceptible to dissipation for higher longitudinal pitch distances L_p. Even though they locally increase heat transfer at the fin leading edge, they have a minor impact on global heat transfer enhancement compared to the main longitudinal vortices.

Induced vortices

Fig. 12 shows the induced vortices. The induced vortices form due to the free shear between the main longitudinal vortices and the flow along the walls. Depending on the geometrical configuration, these vortices vary in size and strength and so do their impact on heat transfer enhancement.

4.2. Effect of longitudinal pitch distance

It is evident from Fig. 13 and 14 that the impact of the corner vortices downstream decrease as the longitudinal pitch distance increase. For $L_\mathrm{p}/H = 0.3$ the corner vortices persist all the way to the following winglet pair. This yields a higher pressure loss due to their interaction with the following winglet pair and also a higher heat transfer enhancement due to the enhanced mixing in the high temperature region near the lower wall. Furthermore, for the lower longitudinal pitch distances, the main longitudinal vortices do not have time to develop before reaching the next winglet pair. This yields a region with smaller lower wall temperature gradients compared to the configurations with higher longitudinal pitch distances as shown in Fig. 14. Therefore, the heat transfer enhancement relative to the pressure loss increase is low. This is in agreement with global tendencies depicted in Fig. 9 and 10. The same tendency applies to the main longitudinal vortices and induced vortices i.e. that the impact on heat transfer enhancement and pressure loss decrease with increasing longitudinal pitch distance. This is due to the increased dissipation of the vortices as they travel further downstream before reaching the following winglet pairs. Therefore, the bound-

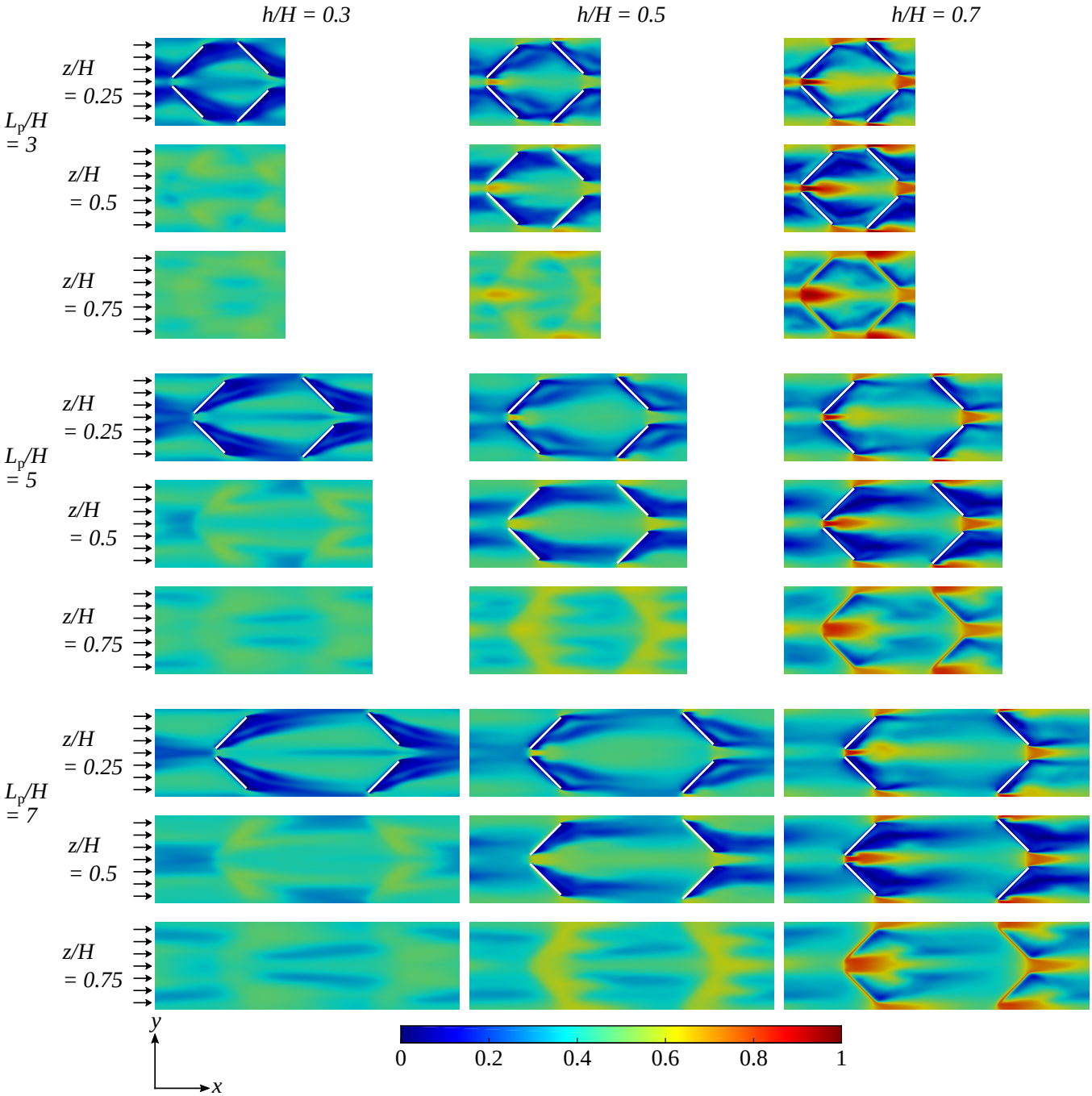

Fig. 13. Time-averaged velocity magnitude in the xy-plane normalised by the maximum time-averaged velocity for the configurations $\langle|u|\rangle/\max\langle|u|\rangle$. Three longitudinal pitch distances L_p/H and winglet heights h/H are shown. Each configuration is shown at z-positions of $z/H = 0.25$, $z/H = 0.50$ and $z/H = 0.75$.

ary layer to core flow mixing occurs over a shorter distance which yields a lower overall heat transfer enhancement.

4.3. Effect of winglet height

As mentioned earlier, variations in winglet height greatly affects both heat transfer and pressure loss. When considering heat transfer it is evident from Fig. 14 that higher temperature gradients at the lower wall are generally observed for smaller winglet heights. At larger winglet heights there is a more even distribution between the upper and lower walls. This is attributed to the generation of larger and stronger main longitudi-

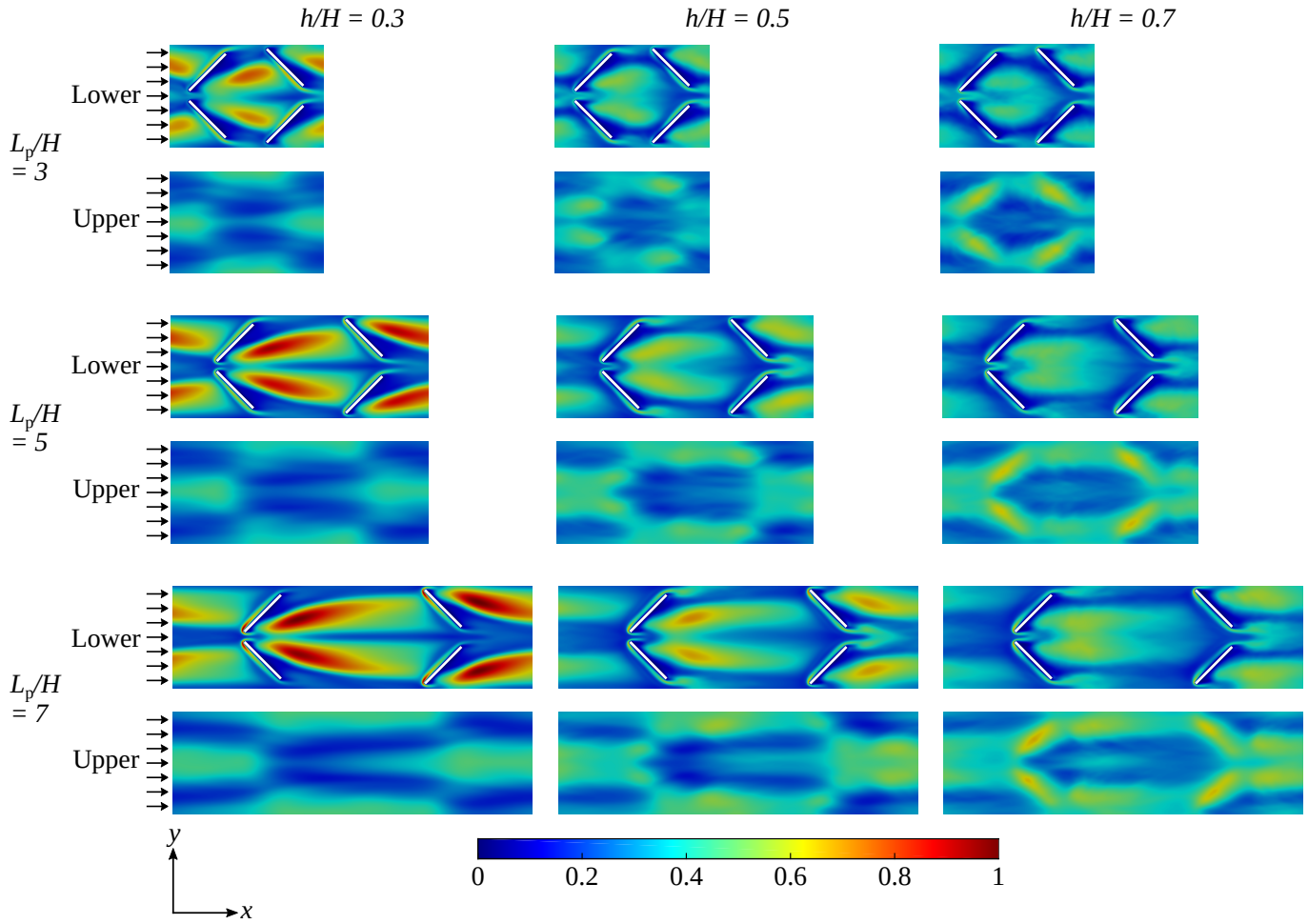

Fig. 14. Time-averaged wall normal temperature gradient for the lower $z/H = 0$ and upper wall $z/H = 1$ normalised by the maximum wall temperature gradient for the configurations $\langle|\partial T/\partial n|\rangle/\max\langle|\partial T/\partial n|\rangle$. Three longitudinal pitch distances L_p/H and winglet heights h/H are shown.

nal, corner and induced vortices and to the increased flow rate being forced around and above the higher winglet due to increased channel blockage. Overall, this leads to a higher heat transfer enhancement for the higher winglet as also shown in Fig. 9. Furthermore, since the vortices are larger in size they are more susceptible to dissipation. This is in agreement with the fact that the longitudinal pitch distance does have a higher impact on the heat transfer enhancement as the winglet height increases. However, for $h/H = 0.3$ Fig. 14 shows that a region with high wall temperature gradients is persistent downstream along the lower wall. This suggests that the smaller main longitudinal vortices generated by the lower winglets are less susceptible to dissipation and therefore provide a more stable heat transfer enhancement downstream. Furthermore, lower winglet heights result in a significantly smaller form drag, which can be visualised indirectly by the lower velocities around the winglets in Fig. 13. In agreement with Fig. 11, this suggests optimum configurations to have a combination of lower winglet heights and higher longitudinal pitch distances.

5. Conclusion

The present study numerically investigates the effect of changes in winglet height and longitudinal pitch distance on heat transfer and pressure loss in repeating arrangements of staggered rectangular winglet pairs inserted into a channel with height H and bulk velocity u_b. Large Eddy Simulations are performed for $\mathrm{Re} = u_\mathrm{b}H/\nu = 700$

and Pr = 0.71 on a periodic section of the geometry to map how the geometrical variations affect Nusselt number Nu, loss coefficient f and the performance factor $\eta = (\mathrm{Nu}/\mathrm{Nu}_0)/(f/f_0)^{1/3}$. The winglet height h and longitudinal pitch distance L_p are varied in the ranges $h/H \in [0.3; 0.7]$ and $L_\mathrm{p}/H \in [3.0; 7.0]$ with step sizes of 0.1 and 1.0 respectively.

The flow structures generated by the rectangular winglet pair vortex generators can be categorised in three distinctive types of vortices: main longitudinal vortices, corner vortices and induced vortices. The main longitudinal vortices are found to play a major role for heat transfer enhancement due to their interaction with the thermal boundary layer leading to a high degree of boundary layer to core flow mixing. There is a positive relation between the size and strength of the main longitudinal vortices and the winglet height, while their persistence downstream decrease with increasing size and strength. This is due to the fact that the larger longitudinal vortices, yielding a higher degree of interaction with the upper and lower thermal boundary layer, are subjected to an increased dissipation. Therefore, the heat transfer enhancement is more sensitive to changes in the longitudinal pitch distance for higher winglet heights. The pressure loss shows the same tendency. Overall, pressure loss increments f/f_0 ranging between 3.3 and 33.5 and heat transfer enhancements $\mathrm{Nu}/\mathrm{Nu}_0$ ranging between 2.2 and 4.6 are found.

When combining heat transfer and pressure loss in the performance factor η describing heat transfer enhancement relative to the pressure loss, the optimum configuration is found at lower winglet heights and higher longitudinal pitch distances. At the lower winglet heights, the main longitudinal vortices persists longer downstream, which leads to a more uniform heat transfer enhancement through the channel at a reasonable pressure loss.

Furthermore, the results show that local heat transfer can effectively be directed to either side by geometrical variations. Lower winglet heights generally result in high local heat transfer on the fin side. Additionally, if a higher pressure loss increase is tolerable, a higher winglet height and smaller longitudinal pitch should generally be considered. Therefore, depending on the exact application, the results in this study may be used to help the design process.

Further studies could focus on a direct comparison with an aligned arrangement of rectangular winglet vortex generators in the same configuration as used in the present study. Even though studies exist in literature no direct comparisons exist to the authors knowledge. Furthermore, an expansion of the geometrical parametric variations conducted in this study is suggested for future studies. It is suggested that the staggered offset is varied to determine whether the performance would change if the vortices are not interrupted due to the following winglet pair being almost right behind the first pair. Furthermore, the winglet aspect ratio could be varied to determine whether a high or lower aspect ratio wing would perform better or worse. This is especially important for cases where the fin temperature cannot be considered constant.

Acknowledgements

Simulations were done using OpenFOAM 3.0.x modified to solve Eq. (1) and (2) on the Abacus 2.0 cluster located at the DeIC National HPC Centre, University of Southern Denmark (SDU).

References

[1] A. Sohankar, L. Davidson, Effect of inclined vortex generators on heat transfer enhancement in a three-dimensional channel, Numerical Heat Transfer, Part A: Applications 39 (5) (2001) 433–448, doi: 10.1080/10407780121572.

[2] M. Awais, A. A. Bhuiyan, Heat transfer enhancement using different types of vortex generators (VGs): A review on experimental and numerical activities, Thermal Science and Engineering Progress 5 (2018) 524–545, doi:10.1016/j.tsep.2018.02.007.

[3] T. Alam, M.-H. Kim, A comprehensive review on single phase heat transfer enhancement techniques in heat exchanger applications, Renewable and Sustainable Energy Reviews 81 (1) (2018) 813 – 839, doi: 10.1016/j.rser.2017.08.060.

[4] A. Jacobi, R. Shah, Heat transfer surface enhancement through the use of longitudinal vortices: A

review of recent progress, Experimental Thermal and Fluid Science 11 (3) (1995) 295–309, doi: 10.1016/0894-1777(95)00066-U.

[5] G. Biswas, N. K. Mitra, M. Fiebig, Computation of Laminar Mixed Convection Flow in a Channel with Wing Type Built-in Obstacles, Journal of Thermophysics and Heat Transfer 3 (4) (1989) 447–453, doi: 10.2514/3.28769.

[6] G. Biswas, H. Chattopadhyay, Heat transfer in a channel with built-in wing-type vortex generators, International Journal of Heat and Mass Transfer 35 (4) (1992) 803–814, doi:10.1016/0017-9310(92)90248-Q.

[7] S. Tiggelbeck, N. Mitra, M. Fiebig, Flow structure and heat transfer in a channel with multiple longitudinal vortex generators, Experimental Thermal and Fluid Science 5 (4) (1992) 425–436, doi:10.1016/0894-1777(92)90029-5.

[8] S. Tiggelbeck, N. Mitra, M. Fiebig, Experimental investigations of heat transfer enhancement and flow losses in a channel with double rows of longitudinal vortex generators, International Journal of Heat and Mass Transfer 36 (9) (1993) 2327–2337, doi: 10.1016/S0017-9310(05)80117-6.

[9] S. Tiggelbeck, N. K. Mitra, M. Fiebig, Comparison of Wing-Type Vortex Generators for Heat Transfer Enhancement in Channel Flows, Journal of Heat Transfer 116 (4) (1994) 880–885, doi:10.1115/1.2911462.

[10] F. Edwards, G. Alker, The Improvement of Forced Convection Surface Heat Transfer Using Surface Protrusions in the Form of (A) Cubes and (B) Vortex Generators, in: Proceedings of the Fifth International Heat Transfer Conference in Tokyo, vol. 2, 2244–2248, 1974.

[11] K. Torii, J. Yanagihara, The Effects of Longitudinal Vortices on Heat Transfer of Laminar Boundary Layers, JSME international journal 32 (3) (1989) 395–402, doi:10.1299/jsmeb1988.32.3_395.

[12] M. C. Gentry, A. M. Jacobi, Heat Transfer Enhancement by Delta-Wing-Generated Tip Vortices in Flat-Plate and Developing Channel Flows, Journal of Heat Transfer 124 (6) (2002) 1158–1168, doi: 10.1115/1.1513578.

[13] A. Sohankar, Heat transfer augmentation in a rectangular channel with a vee-shaped vortex generator, International Journal of Heat and Fluid Flow 28 (2) (2007) 306–317, doi: 10.1016/j.ijheatfluidflow.2006.03.002.

[14] S. Ferrouillat, P. Tochon, C. Garnier, H. Peerhossaini, Intensification of heat-transfer and mixing in multifunctional heat exchangers by artificially generated streamwise vorticity, Applied Thermal Engineering 26 (16) (2006) 1820–1829, doi: 10.1016/j.applthermaleng.2006.02.002.

[15] J. M. Wu, W. Q. Tao, Numerical study on laminar convection heat transfer in a rectangular channel with longitudinal vortex generator. Part A: Verification of field synergy principle, International Journal of Heat and Mass Transfer 51 (5) (2008) 1179–1191, doi:10.1016/j.ijheatmasstransfer.2007.03.032.

[16] J. M. Wu, W. Q. Tao, Numerical study on laminar convection heat transfer in a channel with longitudinal vortex generator. Part B: Parametric study of major influence factors, International Journal of Heat and Mass Transfer 51 (13) (2008) 3683–3692, doi: 10.1016/j.ijheatmasstransfer.2007.03.031.

[17] M. Fiebig, Vortices, Generators and Heat Transfer, Chemical Engineering Research and Design 76 (2) (1998) 108–123, doi:10.1205/026387698524686, 5th UK National Heat Transfer Conference.

[18] A. Abdollahi, M. Shams, Optimization of shape and angle of attack of winglet vortex generator in a rectangular channel for heat transfer enhancement, Applied Thermal Engineering 81 (2015) 376–387, doi: 10.1016/j.applthermaleng.2015.01.044.

[19] M. Fiebig, Vortices and Heat Transfer, Journal of Applied Mathematics and Mechanics 77 (1) (1997) 3–18, doi:10.1002/zamm.19970770103.

[20] C. Liu, J. tong Teng, J.-C. Chu, Y. lang Chiu, S. Huang, S. Jin, T. Dang, R. Greif, H.-H. Pan, Experimental investigations on liquid flow and heat transfer in rectangular microchannel with longitudinal vortex generators, International Journal of Heat and Mass Transfer 54 (13) (2011) 3069–3080, doi: 10.1016/j.ijheatmasstransfer.2011.02.030.

[21] F. Dupont, C. Gabillet, P. Bot, Experimental Study of the Flow in a Compact Heat Exchanger Channel With Embossed-Type Vortex Generators, Journal of Fluids Engineering 125 (4) (2003) 701–709, doi: 10.1115/1.1595675.

[22] A. Akcayoglu, Flow past confined delta-wing type vortex generators, Experimental Thermal and Fluid Science 35 (1) (2011) 112–120, doi: 10.1016/j.expthermflusci.2010.08.012.

[23] J. X. Zhu, N. K. Mitra, M. Fiebig, Effects of longitudinal vortex generators on heat transfer and flow loss in turbulent channel flows, International Journal of Heat and Mass Transfer 36 (9) (1993) 2339–2347, doi:10.1016/S0017-9310(05)80118-8.

[24] C. M. B. Russell, T. V. Jones, G. H. Lee, Heat transfer enhancement using vortex generators, in: Proceedings of the Seventh International Heat Transfer Conference, vol. 3, 283–288, 1982.

[25] A. Sinha, K. A. Raman, H. Chattopadhyay, G. Biswas, Effects of different orientations of winglet arrays on the performance of plate-fin heat exchangers, International Journal of Heat and Mass Transfer 57 (1) (2013) 202–214, doi: 10.1016/j.ijheatmasstransfer.2012.10.034.

[26] L.-T. Tian, Y.-L. He, Y.-G. Lei, W.-Q. Tao, Numerical study of fluid flow and heat transfer in a flat-plate channel with longitudinal vortex generators by applying field synergy princi-

ple analysis, International Communications in Heat and Mass Transfer 36 (2) (2009) 111–120, doi: 10.1016/j.icheatmasstransfer.2008.10.018.

[27] Y. Chen, M. Fiebig, N. Mitra, Heat transfer enhancement of finned oval tubes with staggered punched longitudinal vortex generators, International Journal of Heat and Mass Transfer 43 (3) (2000) 417–435, doi: 10.1016/S0017-9310(99)00157-X.

[28] A. Y. Turk, G. H. Junkhan, Heat transfer enhancement downstream of vortex generators on a flat plate, in: Proceedings of the Eighth International Heat Transfer Conference, vol. 6, 2903–2908, 1986.

[29] H.-Y. Li, C.-L. Chen, S.-M. Chao, G.-F. Liang, Enhancing heat transfer in a plate-fin heat sink using delta winglet vortex generators, International Journal of Heat and Mass Transfer 67 (2013) 666–677, doi:10.1016/j.ijheatmasstransfer.2013.08.042.

[30] S. V. Patankar, C. H. Liu, E. M. Sparrow, Fully Developed Flow and Heat Transfer in Ducts Having Streamwise-Periodic Variations of Cross-Sectional Area, Journal of Heat Transfer 99 (2) (1977) 180–186, doi:10.1115/1.3450666.

[31] J. Hærvig, T. J. Condra, K. Sørensen, On the fully-developed heat transfer enhancing flow field in sinusoidally, spirally corrugated tubes using computational fluid dynamics, International Journal of Heat and Mass Transfer 106 (2017) 1051–1062, doi: 10.1016/j.ijheatmasstransfer.2016.10.080.

[32] L. Davidson, Large Eddy Simulations: How to evaluate resolution, International Journal of Heat and Fluid Flow 30 (5) (2009) 1016–1025, doi: 10.1016/j.ijheatfluidflow.2009.06.006.

[33] M. Mirzaei, A. Sohankar, L. Davidson, F. Innings, Large Eddy Simulation of the flow and heat transfer in a half-corrugated channel with various wave amplitudes, International Journal of Heat and Mass Transfer 76 (2014) 432–446, doi: 10.1016/j.ijheatmasstransfer.2014.04.018.

[34] F. Nicoud, F. Ducros, Subgrid-Scale Stress Modelling Based on the Square of the Velocity Gradient Tensor, Flow, Turbulence and Combustion 62 (3) (1999) 183–200, doi:10.1023/A:1009995426001.

[35] A. Esmaeilzadeh, N. Amanifard, H. Deylami, Comparison of simple and curved trapezoidal longitudinal vortex generators for optimum flow characteristics and heat transfer augmentation in a heat exchanger, Applied Thermal Engineering 125 (2017) 1414 – 1425, doi:10.1016/j.applthermaleng.2017.07.115.

[36] R. L. Webb, E. R. G. Eckert, Application of rough surfaces to heat exchanger design, International Journal of Heat and Mass Transfer 15 (9) (1972) 1647–1658, doi:10.1016/0017-9310(72)90095-6.

[37] P. J. Roache, Perspective: A Method for Uniform Reporting of Grid Refinement Studies, Journal of Fluids Engineering 116 (3) (1994) 405–413, doi: 10.1115/1.2910291.

Nomenclature

Roman symbols

A	Cross-sectional area (m^2)
$\boldsymbol{A}$	Face normal vector (-)
B_o	Staggered offset (m)
B_p	Transverse pitch distance (m)
$\boldsymbol{c}$	Vector from cell centre to cell centre of adjacent face sharing cell (-)
c_p	Specific heat capacity (J kg^{-1} K^{-1})
C_ω	WALE constant (-)
e	Winglet pair tip distance (m)
f	Loss coefficient (-)
$\boldsymbol{f}$	Vector from cell centre to face centre (-)
f_e	Estimated exact solution of f (-)
F_s	Safety factor (-)
h	Winglet height (m)
H	Domain height (m)
l	Winglet length (m)
L_d	Domain length (m)
L_p	Longitudinal pitch distance (m)
Nu	Nusselt number (-)
p	Order of convergence (-)
P	Pressure (m^2 s^{-2})
Pr	Prandtl number (-)
Pr_t	Turbulent Prandtl number (-)
$\dot{q}$	Wall heat flux (W m^{-2})
r	Grid refinement ratio (-)
Re	Reynolds number, $Re = u_b H/\nu$ (-)
t	Time (s)
t_w	Winglet thickness (m)
T	Temperature (K)
u	Velocity (m s^{-1})
y^+	Dimensionless wall distance (-)

Greek symbols

α	Angle of attack (-)
β	Streamwise pressure gradient (m s^{-2})
γ	Streamwise temperature gradient (K m^{-1})
δ	Kronecker delta (-)
Δ	Difference (-)
ϵ	Relative error (-)
η	Performance factor (-)
θ_e	Angle of equiangular face/cell (-)
ν	Kinematic viscosity (m^2 s^{-1})
ν_t	Eddy viscosity (m^2 s^{-1})
ρ	Density (kg m^{-3})

Subscripts	
0	Reference
b	Bulk
i	x, y, z-component and i'th entry
j	x, y, z-component and j'th entry
w	Wall
x, y, z	Cartesian coordinate directions
Notation	
$\bar{x}$	Space-filtered
$\langle x \rangle$	Time-averaged
$\lvert x \rvert$	Magnitude
Acronyms	
LES	Large Eddy Simulation
GCI	Grid Convergence Index
PISO	Pressure-Implicit with Splitting of Operators
sgs	Subgrid-scale
WALE	Wall-Adapting Local Eddy-viscosity